ELSEVIER
Engineering Geology 56 (2000) 47–62
ENGINEERING GEOLOGY
www.elsevier.nl/locate/enggeo

Stress estimated using microseismic clusters and its relationship to the fracture system of the Hijiori hot dry rock reservoir

K. Tezuka [a,*], H. Niitsuma [b]

[a] *JAPEX Research Center, 1-2-1 Hamada, Mihama-ku, Chiba City 261-0025, Japan*
[b] *Tohoku University, 01 Aoba, Aramaki, Aoba-ku, Sendai City 980-8599, Japan*

Abstract

A method for estimating the in situ stress state by analyzing microseismic clusters induced by hydraulic injections is proposed. The method is based on focal mechanism analysis, supplemented with microseismic doublet analysis. The latter is used to discriminate between the fault plane and the auxiliary planes of the focal mechanism solution. The method was applied to estimate the stress field within the Hijiori hot dry rock geothermal reservoir and yielded results which were consistent with other estimates. The mechanics of permeability creation within the reservoir during major hydraulic injections was then examined by evaluating the interaction of the inferred stress field with the natural fracture system. The characteristics of the latter were determined by integrating information obtained from core samples, acoustic borehole televiewer images and pressure, temperature and spinner logs. The results indicated that the observed microseismicity and orientation-dependent permeability characteristics of the fracture population are well explained by shear failure inferred from Coulomb's friction theory. It is also shown that the growth direction of the reservoir is strongly controlled by the distribution of favorably oriented pre-existing fractures and their interaction with the stress field.

Keywords: Doublet; Focal mechanism; Fracture; Hijiori; Hot Dry Rock; Microseismic; Multiplet; Stress

1. Introduction

The hot dry rock (HDR) concept of geothermal exploitation, as illustrated in Fig. 1, involves drilling two or more wells to a suitable depth, creating a 'reservoir' of permeable, fractured rock, and pumping cold water into the reservoir through an injection borehole. The injected water heats up as it flows through the reservoir and is pumped to the earth's surface through a second borehole, the production well, where the heat is extracted (Parker, 1989). Since 1984 the New Energy and Industrial Technology Development Organization (NEDO) Japan has been conducting a HDR geothermal project at the Hijiori test site, located near Yamagata, Japan. In 1992, a reservoir was created in the granodiorite basement rock ca. 2200 m depth by injecting 2100 m^3 of fluid at surface pressures as high as 26 MPa. This succeeded in establishing a fluid circulation system between one injection well (HDR-1) and two production wells (HDR-2a, HDR-3). Microseismicity was monitored throughout this and several subsequent hydraulic tests.

* Corresponding author. Tel.: +0081-22-217-7398; fax: +81-22-217-7398.
E-mail addresses: tezuka@rc.japex.co.jp (K. Tezuka), ni@ni4.earth.tohoku.ac.jp (H. Niitsuma)

PII: S0013-7952(99)00133-7

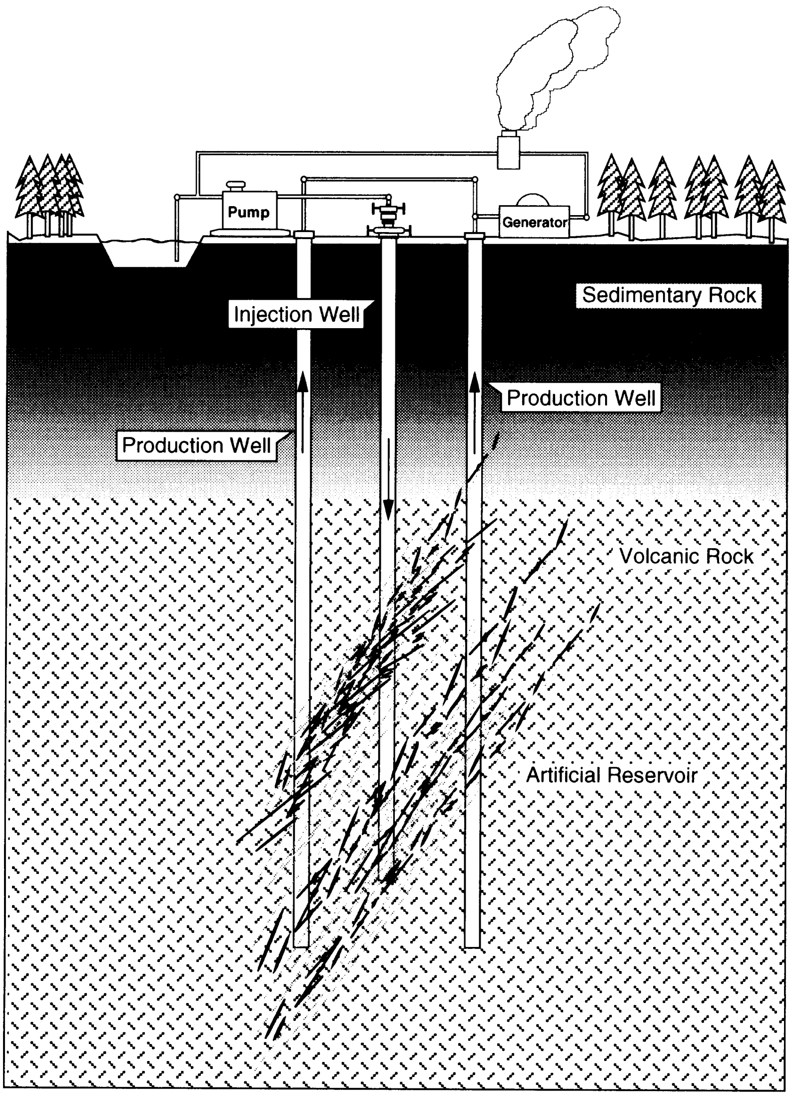

Fig. 1. Concept of the HDR geothermal energy extraction system.

These data were supplemented by various types of borehole logs such as acoustic borehole televiewer (referred to as BHTV), pressure, temperature and spinner flow meter logs (referred to as PTS logs). The collective data indicated that the created reservoir consisted of natural and stimulated natural fractures. The fractures define a network within which the flow paths, heat exchange surfaces and storage spaces for hot water in the reservoir are contained. The fractures, which act as flow paths, are particularly important since they play a vital role in determining the reservoir characteristics and performance. The contemporary stress field prevailing over the reservoir is also believed to be a primary factor controlling the fluid flow through its interaction with the natural fracture system. The relationship between hydraulically-conductive fractures and stress state has been investigated by several researchers (Pine and Batchelor, 1984; Sibson, 1996; Barton et al., 1997). These studies emphasize the importance of stress in controlling the dominant flow direction and the direction of reservoir growth during reservoir creation. The successful development of a HDR reservoir depends on a judicious choice of site based upon careful preliminary characterization of natural fractures and stress state within the prospective reservoir.

In this paper, the stress state and its relationship to the fracture system in the Hijiori HDR reservoir is investigated. First, we briefly describe the Hijiori HDR test site and present the microseismic events clusters observed during the hydraulic injections. Next, we propose a method to estimate the contemporary in situ stress field by using microseismic event clusters and applied it to the Hijiori microseismic data. Finally we discuss the development of the Hijiori HDR reservoir by integrating the stress estimates with information on the fracture network derived from oriented cores, BHTV images and PTS logs.

2. Hijiori hot dry rock test site

Hijiori is in the Yamagata prefecture which is located at the northern part of Honshu Island, Tohoku district in Japan (Fig. 2). The topography is characterized by a volcanic depression called a caldera, whose diameter is ca. 1.5–2 km. The test site is at southern rim of the caldera where four boreholes (HDR-1, HDR-2a, HDR-3 and SKG-2) have been drilled to between 1800 and 2300 m depth. The geologic basement in and around the Hijiori area is composed of a cretaceous granodiorite which has been widely altered by hydrothermal processes. According to the geological data from the wells drilled at this site, there are seven major

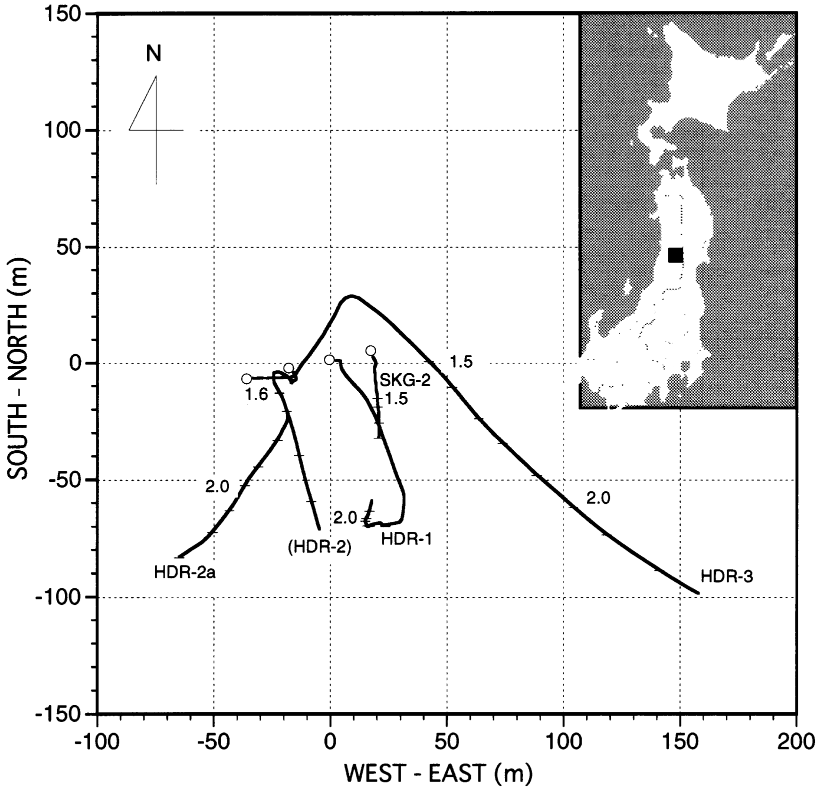

Fig. 2. Location of the Hijiori test site showing the trajectories of the wells HDR-1, HDR-2a, HDR-3 and SKG-2

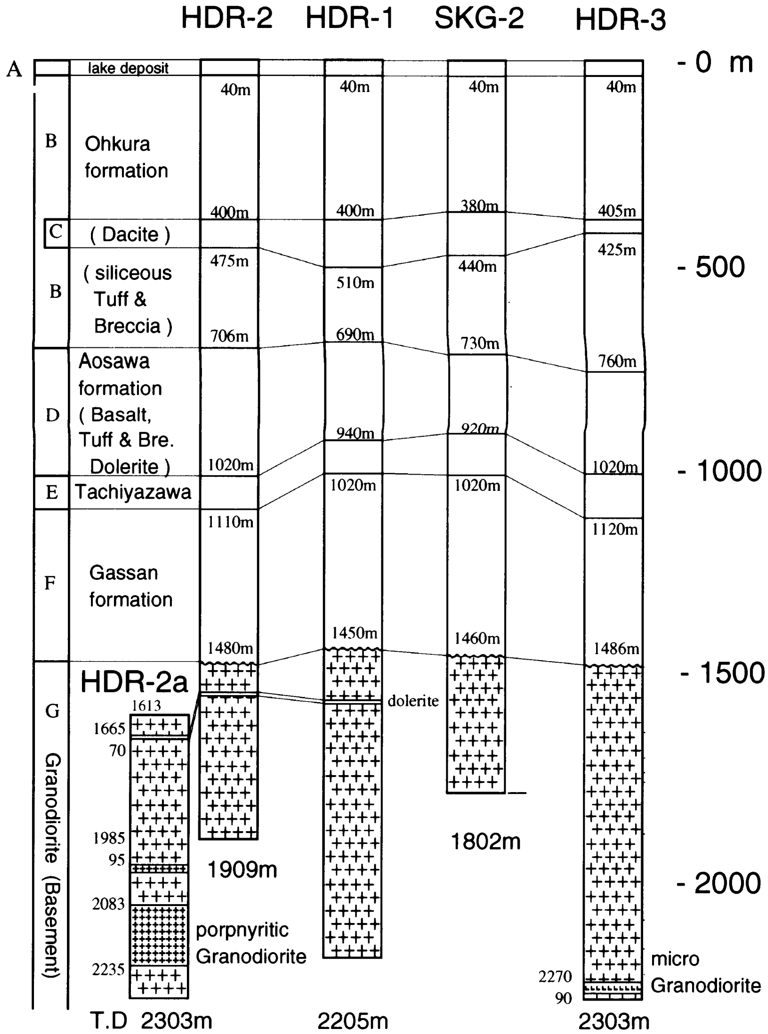

Fig. 3. Stratigraphic column of the wells drilled in the Hijiori test site.

rock units. These are shown in Fig. 3 and are as follows: a pyroclastic flow deposit (A); the miocene Ohkura siliceous tuff formation (B); a dacite lava and hydroclastite (C); the Aosawa formation consisting of flood type basalt lava, a sheet and dyke type dolerite (D), the Tachiyazawa formation consisting of tuff, tuffeceous sandstone and mudstone (E); the Gassan formation which consists of Neogene basaltic and andestic lava, breccia and volcanic conglomerate (F); and the granodiorite basement which unconformably underlies the Gassan (Kitani et al., 1998). Aerophotography lineament and topographic surveys show the existence of many faults around the rim of caldera that form a roughly polygonal shape. The reservoir was created in the basement at ca. 2200 m depth.

3. Microseismic clusters

The microseismic events analyzed in this paper were induced during two experiments. One was the ‘hydraulic fracturing’ experiment of 1992 (exp. 9202) in which a total of 2100 m^3 of water was injected into HDR-1 at a maximum rate of 72 kg s^{-1} and a peak wellhead pressure of 26 MPa. The other was a 1 month hydraulic circulation test performed in 1995 (exp. 9502) in which HDR-1 was used as an injection well at a maximum rate of 57 kg s^{-1} and peak wellhead pressure of 15 MPa. Production was from both HDR-2a and HDR-3. During the two experiments, >2000 microseismic events were recorded. A detailed inspection of the waveforms of the events revealed the presence of subsets of events which produced a similar waveform at all observation stations. These events are referred to in the literature as microseismic doublets or multiplets. Members of a multiplet generally occur close together so as to define a cluster, and have similar focal mechanisms (Poupinet et al., 1984; Moriya et al., 1994; Phillips et al., 1997). Because of the waveform similarity of multiplets, a precise relative-location analysis can be performed on the sources using a cross correlation technique. Fig. 4 shows microseismic event locations estimated by this technique (Tezuka and Niitsuma, 1995). The blue circles and the red circles denote the microseismic event locations observed during the exp. 9202 and exp. 9502, respectively. The lines in the figure represent the well trajectories, and the filled squares along the lines denote producing zones identified by PTS logs during the circulation test in 1995 (exp. 9502). The distribution of events shown in the b′–b cross-section reveals several concentrated clusters which appear to have a good spatial correlation with the producing zones. The upper blue cluster, which includes more than three sub-clusters, crosses the

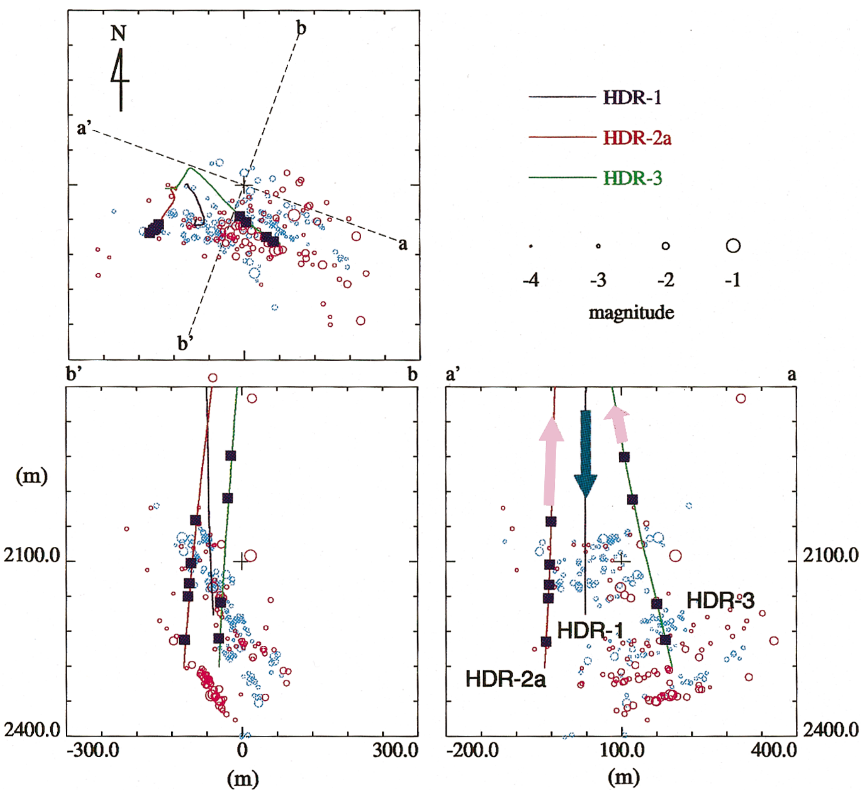

Fig. 4. Distribution of the microseismic events associated with the hydraulic fracturing experiment in 1992 (blue circles) and the hydraulic circulation test in 1995 (red circles) at the Hijiori HDR test site. The source locations were calculated by the technique of microseismic doublet analysis. Upper, plan view; lower, elevation views along the orthogonal cross-section b′–b and a′–a. HDR-1 is the injection well. The black filled symbols along HDR-2a and HDR-3 are production zones estimated by PTS logging during the circulation test.

upper two producing zones of the HDR-2a well and the lower two producing zones of the HDR-3 well. The lower red cluster is situated beneath the bottom of HDR-3 and does not extend as far as borehole HDR-2. By extrapolation, however, the trend of the cluster intersects the lowest production zone of the HDR-2a well. These results provide a basis to propose that the microseismic clusters represent some of major flow paths in the Hijiori HDR reservoir.

4. Stress estimation

Microseismic events represent shear or mixed-mode failure of rocks along pre-existing planes of weakness that is accompanied by significant seismic energy release at relatively high frequencies. In the HDR stimulation, events are usually triggered by raising the pore pressure above levels previously attained (Pine and Batchelor, 1984). Thus, events were predominantly detected during hydraulic stimulations at the Hijiori reservoir. The radiation pattern of the events is generally consistent with that expected for shear failure. The slip direction of failure is controlled by the direction of the plane of weakness and the stress regime. Thus, if the focal mechanisms of microseismic events are known, the inverse problem can be solved to yield information about the state of stress (Gephart and Forsyth, 1984). A fault plane solution of a microseismic event usually provides two possible fault planes which are orthogonal to each other, and it is necessary to identify which

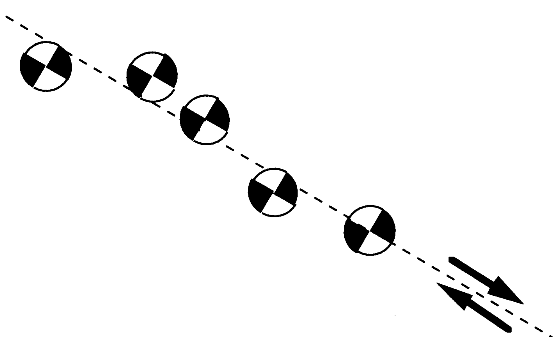

Fig. 5. Expected relationship between the relative locations of the microseismic multiplets and their focal mechanisms.

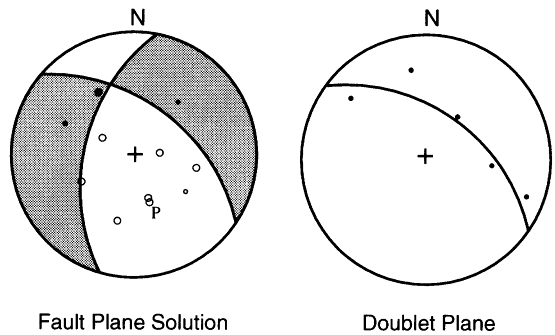

Fig. 6. Comparison of a fault plane solution (a) and a microseismic doublet distribution plane (b). The doublet distribution plane corresponds to one of the nodal planes of the fault plane solution and is thus considered to be the fault plane.

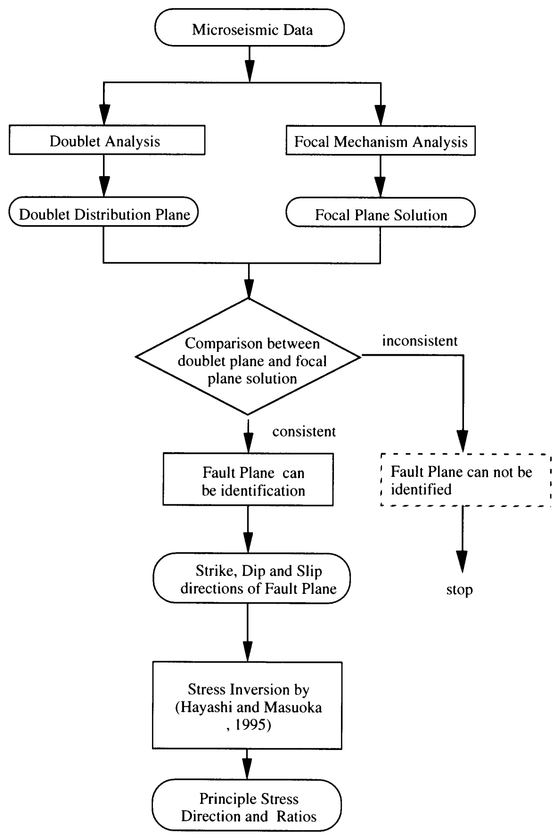

Fig. 7. Flow charts of the method used for estimating the stress field from focal mechanism and microseismic cluster analysis. The method incorporates fault plane solutions and seismic doublet distribution planes into Hayashi and Masoka's (1995) inversion technique.

one is the true failure plane. Multiplet analysis often provides a way of doing this since members of cluster often align along a plane which can be interpreted as a fracture (Augliea et al., 1994). If indeed the events of the multiplet are located on the same plane that has slipped in each of the events, as illustrated in Fig. 5, that plane must be consistent with one of the nodal planes of the fault plane solutions of the events. Fig. 6 shows a comparison of a fault plane solution (left figure) with the associated multiplet distribution plane (right figure) for one multiplet group of the Hijiori data. In the latter, the relative locations of each member of the multiplet group have been projected onto the lower hemisphere of a Wulff net. The arc represents the most likely aligned plane as estimated by a principle component analysis. The nodal plane that dips to the northeast in Fig. 6(a) is almost identical to the multiplet distribution plane of Fig. 6(b). Thus, this plane is considered to be that of the fault. Once the fault plane is identified, the slip direction is also identified from the fault plane solution.

Hayashi and Masoka (1995) proposed a method for estimating principle stress directions and their magnitude ratios by using slip data recorded on fracture surfaces in core samples, assuming that the slip striations are created by frictional slip between two fracture surfaces. The slip directions and the unit normal vectors of the fracture surfaces are used to estimate the stress field. Moriya and Niitsuma (1994) combined this method with a microseismic doublet analysis and used doublet distribution planes as fracture planes. We adapt this technique to our purpose and use the slip directions and the unit normal vectors of the fault planes obtained from microseismic clusters instead of those from core samples. Fig. 7 summarizes the flow chart of the analysis procedure including the technique for microseismic

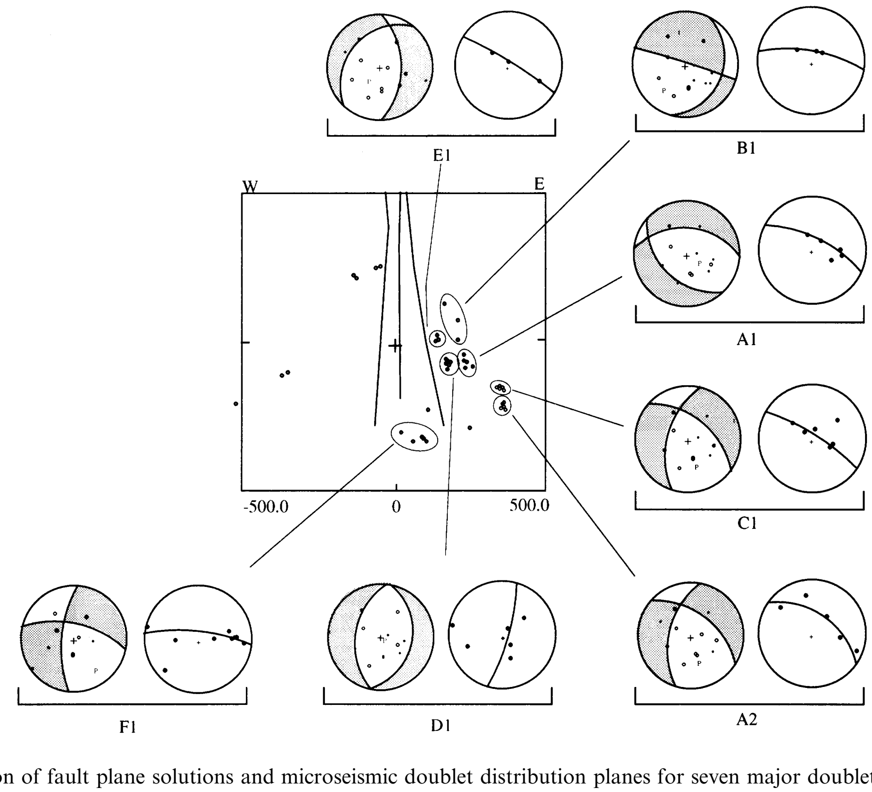

Fig. 8. Comparison of fault plane solutions and microseismic doublet distribution planes for seven major doublet groups. Six of the seven groups (except for group E1) resulted in consistent solutions. This result indicates that the microseismic doublets tend to align on the plane (fracture) which has been activated by hydraulic stimulation.

doublet analysis and Hayashi and Masoka's method.

The proposed method of stress estimation was applied to the Hijiori microseismic data. Fig. 8 shows a comparison of fault plane solutions and multiplet distribution planes for seven major doublet groups. Six of the seven groups resulted in consistent solutions, the exception being group E1. It can be concluded that the microseismic doublets tend to align on the plane (the fracture) which is being activated by the stimulation, and hence that the doublet analysis is useful in identifying the true slip failure planes. Even though the failure planes can be discriminated from the auxiliary planes, there remains some uncertainty in their orientation because the number of stations used for focal mechanism analysis is limited to 10 or 12. Thus, four possible solutions are selected for each doublet group. All possible combinations of these are used in calculating the principle stress directions and the stress deviator. Because the groups A2 and C1 have almost identical solutions, the calculations are performed using five groups (A1, B1, C1, D1 and F1). Eventually 1024 solutions are obtained.

Fig. 9 shows the resulting estimates of the principal stress orientations projected onto a lower hemisphere Wulff net. The maximum principal stress is nearly vertical, and the minimum is sub-horizontal and oriented north–south. The magnitude ratios of the principle stresses are a function of the pore pressure required to induce shear slip. Assuming that the friction coefficient of the fracture surface is 0.8 and the pore pressure during the stimulation is 1.5 times greater than the hydrostatic pressure, the magnitude ratios of principal stresses are calculated to be 1.8:1.2:1.0. The estimates of the orientation of the principal stresses is not affected by pore pressure considerations. The direction of the principal stresses is almost the same as obtained from a conventional inversion technique applied to a number of microseismics focal mechanisms (Sasaki and Kaieda, 1998). It is also roughly consistent with the estimates derived from the inversion of data from drilling induced fractures observed on BHTV images (Okabe et al., 1995).

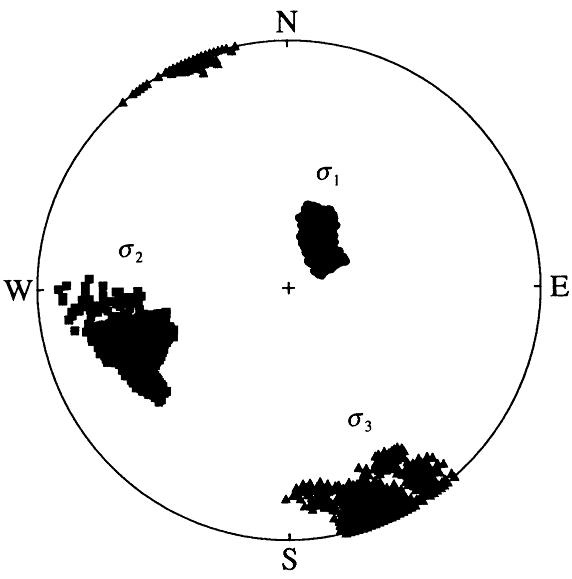

Fig. 9. The principal stress directions estimated by the proposed method using five sets of fault planes and slip directions. The principal stress directions are projected onto a lower hemisphere Wulff net. The maximum principal stress direction is nearly vertical and the minimum principal stress is north–south.

5. Fracture distribution

Fractures along boreholes were investigated using oriented core samples and BHTV images obtained from the wells HDR-2a and HDR-3. The fractures in the oriented core samples were analyzed by scanning the core surface with a contact type core-scanner. Fig. 10 is an example of a scanned core image. As the resolution of the scanned image is <0.1 mm, the technique is able to image relatively small fractures which are not resolved on the BHTV logs. The scanned image includes a few open fractures and many closed or filled small fractures. Some proportion of open fractures are conjugate sets. Although the BHTV image has limited resolution (i.e. it cannot resolve fractures with aperture/alteration zones narrower than ca. 1 mm), it covers most of the borehole and is suitable to investigate the population of relatively larger fractures in a statistical manner. Additionally, a combined analysis with PTS logs provides the possibility of distinguishing the flowing fractures from the others.

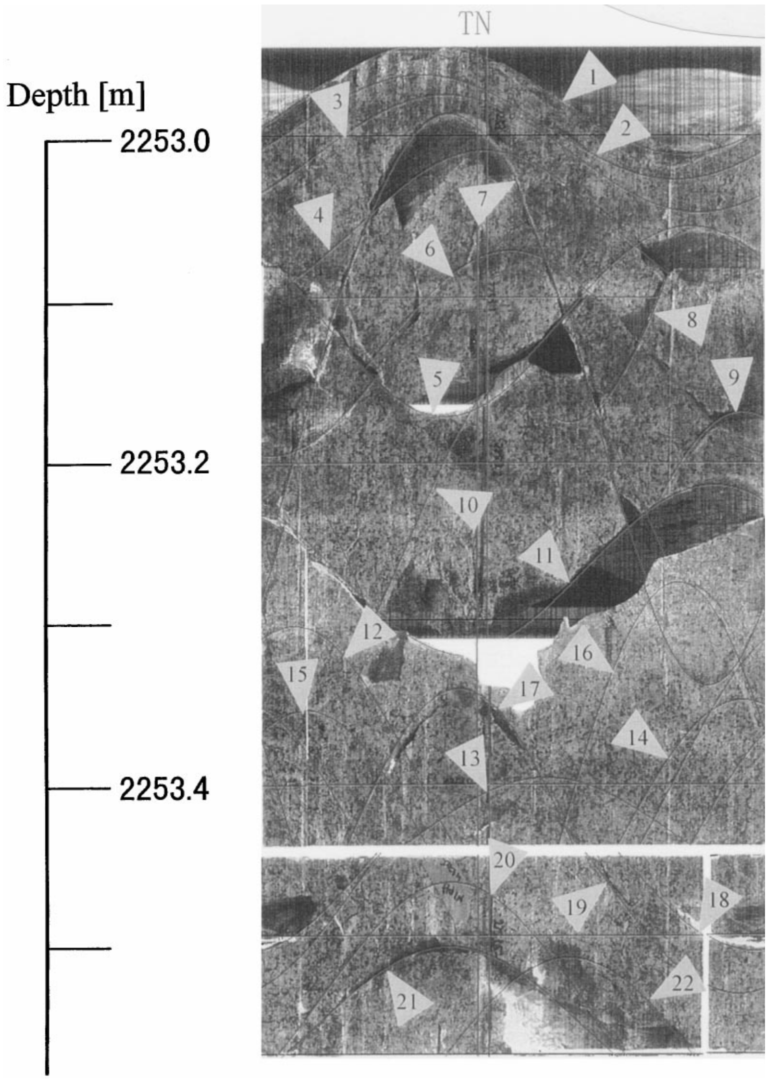

Fig. 10. Example of a scanned image of an oriented core sample. Sinusoidal curves with numbered triangle labels denote the fractures analyzed.

Fig. 11 shows a plot of the azimuth and dip angles of fractures imaged on the BHTV log from HDR-2a. The statistical distribution of fracture orientation and the populations as a function of depth are also plotted as histograms. The north-dipping fractures with high inclination angles are dominant in HDR-2a. This statistical tendency predominates in HDR-2a throughout the depth range 1600–2300 m depth, and is also seen in the HDR-3 well.

Fig. 12 presents a set of plots of poles to fractures projected onto lower hemisphere Wulff nets. Fig. 12(a) shows fractures observed in the oriented cores, Fig. 12(b) shows fractures detected in the BHTV images, and Fig. 12(c) shows the BHTV fractures detected inside and around the production zones as identified from PTS logging. These data are from HDR-2a and HDR-3 within the depth interval 1900–2300 m. The restricted depth range was chosen so as to maintain consis-

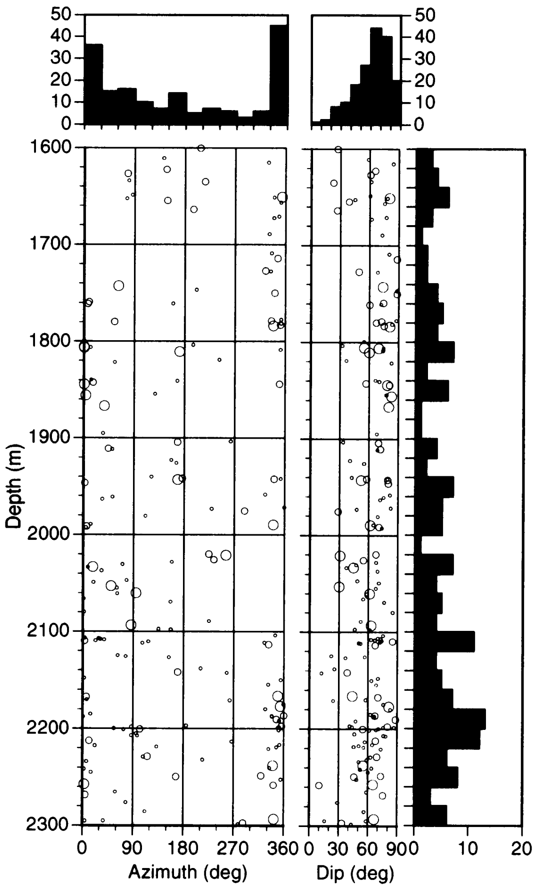

Fig. 11. Plots of dip angle and direction of the fractures detected in BHTV images of the HDR-2a well. The size of the circles reflect the clarity (good, fair, poor) of the fracture on the images. The statistical distribution of fracture orientation and the populations as a function of depth are plotted as histograms. The north dipping fractures with high inclination angles are dominant in the HDR-2a well.

tency with the stress estimates which were derived using microseismic clusters situated below a depth of 1900 m depth. The characteristics of the fracture distributions can be summarized as follows:

1. Fractures dipping to the north with high angles are dominant in both the oriented cores and BHTV images.
2. Fractures dipping to the south at low angles are also seen in the oriented core data, but are less prevalent in the BHTV images.
3. The fractures detected inside and around the production zones are concentrated in a narrow range, even though the total data set contains a wide variation in fractures orientations.

These observations and their implications in the light of the prevailing stress field will be discussed later.

6. Fracture behavior under stressed conditions

Fig. 13 illustrates the behavior of a fracture under a two-dimensional stress condition. σ_1 and σ_3, are the maximum and minimum principle stresses, respectively, and the intermediate principle stress, σ_2, is normal to the paper. θ is the angle between the fracture plane and the minimum stress direction. Three types of stress acting on the fracture surface can be distinguished. These are the normal stress (σ_n), the shear stress (τ), and the static frictional stress. Fig. 13 illustrates the state before pore pressure (p) increased by injection. Static equilibrium prevails when the shear stress in the rock is exactly balanced by the frictional stress at the interface.

Neglecting cohesion, the maximum frictional stress that an interface can support is given from Coulomb friction theory as:

$$\tau_f^{\max} = f_s \sigma_n' \tag{1}$$

where

$$\sigma_n' = \sigma_n - p \tag{2}$$

is the effective normal stress and f_s is the friction coefficient. Thus, during fluid injection the effective normal stress decreases with increases in the pore pressure resulting in a decrease in the peak stress that the interface can support. Hence, at some level of pore pressure increase, shear slip may occur once the peak frictional stress becomes smaller than the shear stress. Thus, on the basis of Coulomb friction theory, we may define an index which measures the proximity of a fracture failure as either effective shear stress or critical pore pressure:

$$\text{effective shear stress: } \tau' = \tau - f_s(\sigma_n - p) \tag{3}$$

$$\text{critical pore pressure: } p_c = \sigma_n - \frac{\tau}{f_s} \tag{4}$$

Reduced effective stress also tends to produce

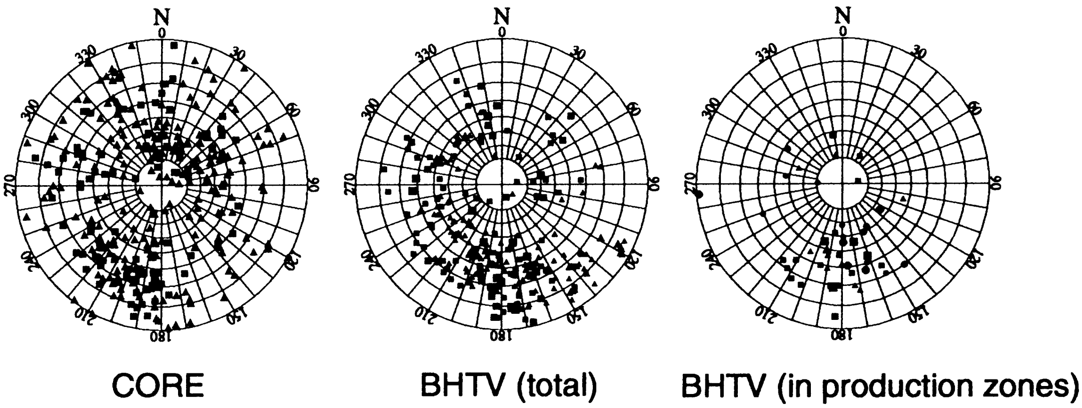

Fig. 12. Plots of fracture poles projected onto a lower hemisphere Wulff nets. (a) Fractures detected in oriented core. (b) Fractures detected in BHTV images. (c) BHTV fractures detected around the production zones. Oriented cores and BHTV data are obtained from the HDR-2a and HDR-3 wells.

fracture dilation (e.g. Walsh and Grosenbaugh, 1979). Thus, we can use the effective normal stress as an index for opening (the fracture walls become completely separated when the effective normal stress fall to zero). These indices are functions of the stress state and the fracture orientation relative to the principal stress directions.

Fig. 14 shows effective normal stress and effective shear stress calculated as functions of fracture angle θ for the case where the maximum principle stress σ_1 is twice as large as the minimum principle stress σ_3. Both calculated stresses have been normalized by σ_3. The five curves correspond to different pore pressures, also normalized by σ_3. The shaded area in Fig. 14(a) identifies stress conditions that can cause the full opening of fractures. Full fracture opening necessarily requires that pore pressure exceed the minimum principal stress, the degree of excess depending upon the fracture angle θ. On the other hand, shear slip may occur for smaller pore pressure increases. This is evident in Fig. 14(b) where the shaded area denotes conditions where the effective shear stress becomes positive and failure occurs. Shear failure is predicted to occur on favorably oriented fractures for pore pressures as low as 0.7 of the minimum stress. This means that for most fracture orientations, conditions which favor shear slip are realized prior to those for opening when pore pressure is gradually increased, such as occurs during a process like a major stimulation injection.

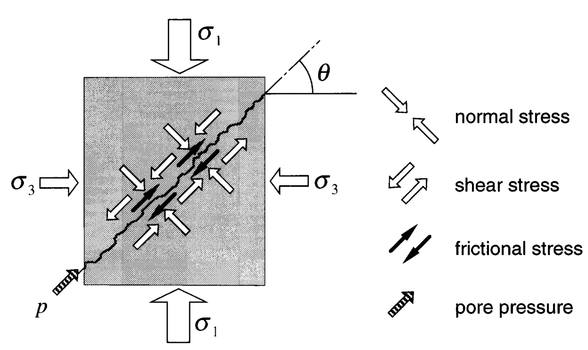

Fig. 13. Diagram illustrating the fracture subjected to a two-dimensional stress condition.

7. Relationship between stress and fracture in the Hijiori reservoir

Applying the Coulomb friction theory described above, we investigated the relationship of the stress field and the orientation distribution of fractures in the Hijiori HDR reservoir. Figs. 15 and 16 show stereographic plots of poles to fractures together with contours of normal stress and the critical pore pressure predicted to act across fractures with such poles. The normal stress and the critical pore pressure were calculated by substituting the nor-

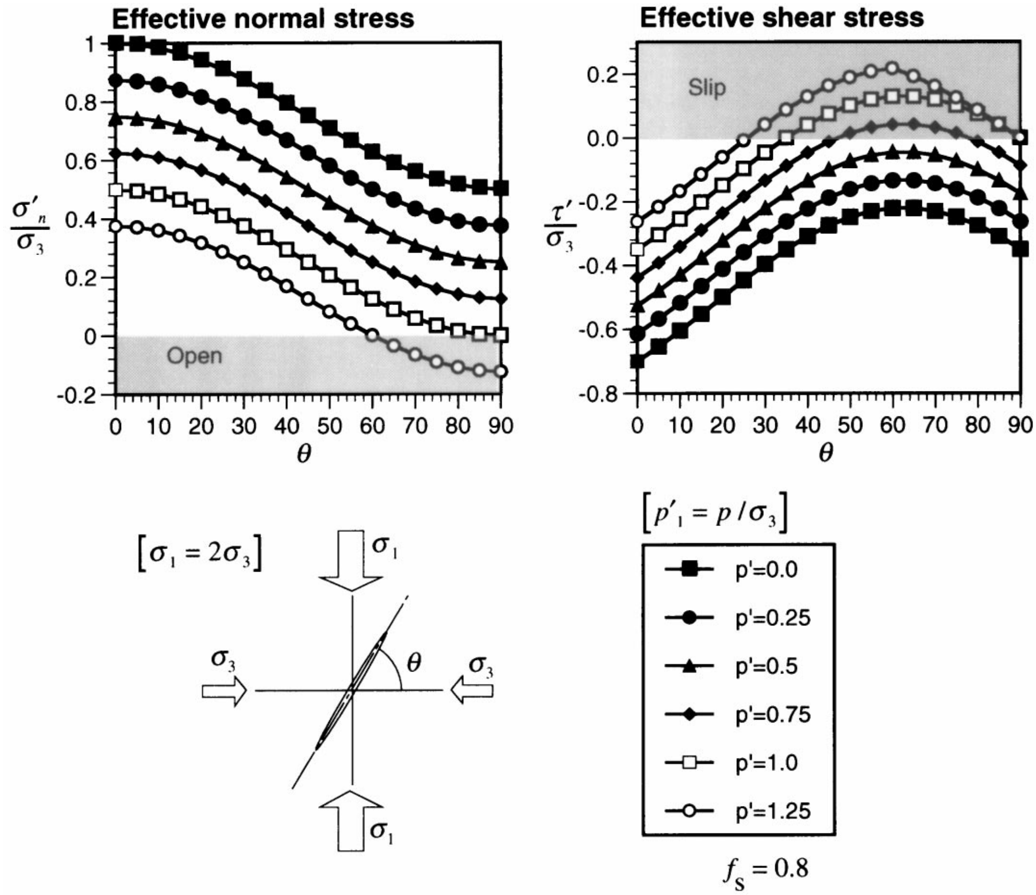

Fig. 14. Plots of effective normal stress (a) and effective shear stress (b) calculated as functions of fracture angle θ and normalized by the minimum stress, σ_3. The meshed area in (a) represents the stress condition expected to produce the full opening of fractures (hydro-jacking). The meshed area in (b) represents the stress condition that would cause shear slip along the fracture assuming a friction coefficient of 0.8. The stress condition for shear slip is reached before that for the opening at most of fracture angles when the pore pressure gradually increases.

malized stress state of the Hijiori reservoir into Eqs. (2) and (4). The red areas in Fig. 15 denote orientations of high normal stress. Fractures whose poles lie in this area are difficult to open. Referring to Fig. 16, the blue areas denote fracture orientations which have relatively low critical pore pressures. Thus, fractures whose poles lie in the blue zones in Fig. 16 are more likely to slip when the pore pressure is increased.

Fig. 15 gives an explanation for the observation that south dipping and shallow-angle fractures are more evident in the cores than in the BHTV images: the poles of these fractures lie in the area where the normal stress is highest and so are the most difficult to open. The fractures and joints in the rock are assumed to be rough surfaces on contact. An apparent aperture of a fracture is due to the height of asperity which is supported by an elastic matrix. The increase in stress normal to the fracture deforms the asperity and compresses the elastic matrix and results in a decrease in the apparent aperture of the fracture (Walsh and Grosenbaugh, 1979). Even if the effective normal stress is positive, the apparent aperture of fracture increases by decreasing normal stress. This might explain why this orientation of fracture could not

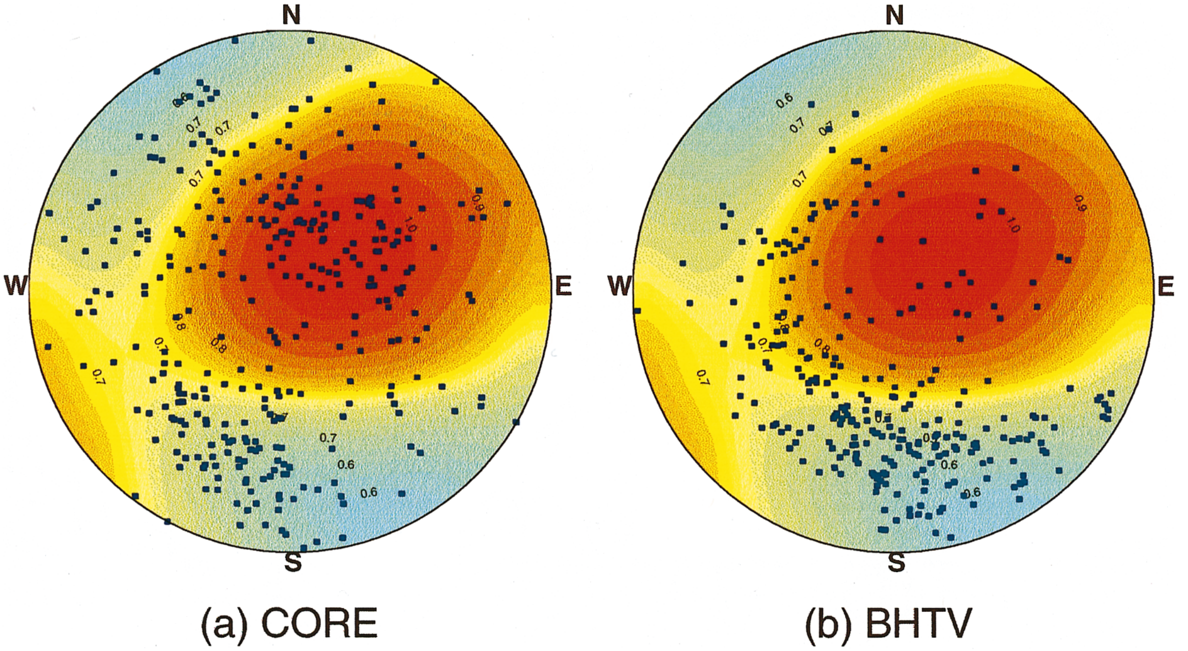

Fig. 15. Contour map of the normal stress acting on fracture surface and the poles of fractures plotted on a lower-hemisphere Wulff net. The stress values have been normalized by the minimum principal stress. The high value area (red area) indicates the orientation in which a fracture is difficult to open. (a) Fractures in oriented cores. (b) Fractures in BHTV images.

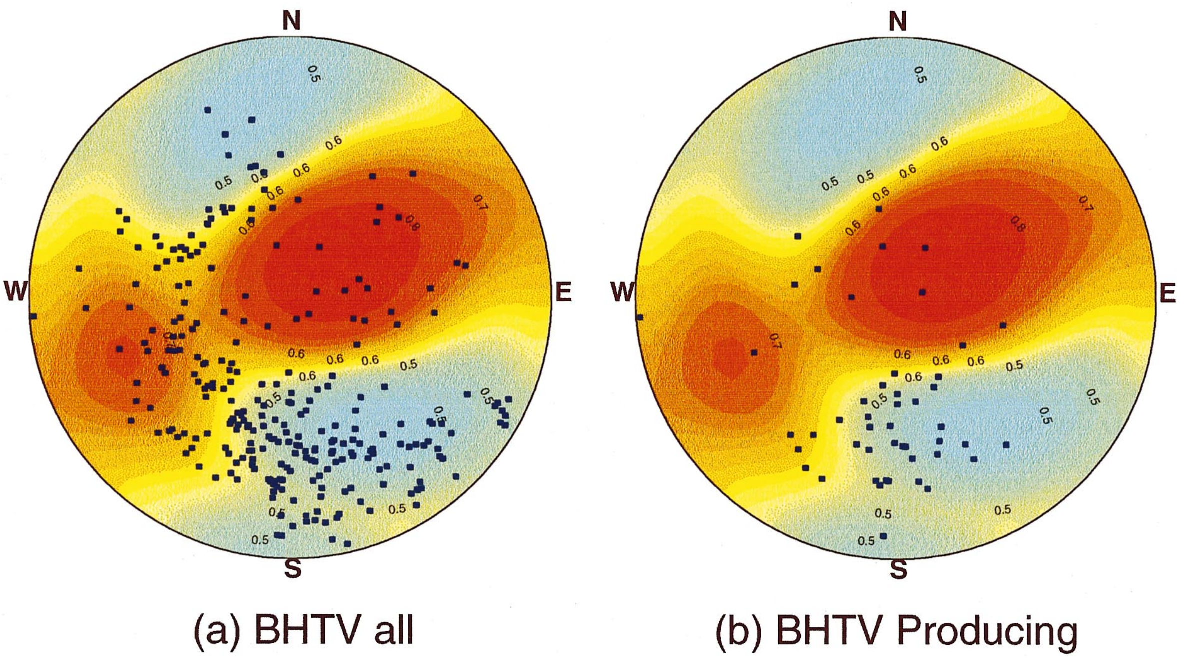

Fig. 16. Contour map of the critical pore pressure and the poles of BHTV fractures detected inside and around the production zones. The low value region (blue area) denotes orientations in which a fracture may slip for comparative small pore pressure increases. (a) All fractures. (b) Fracture detected inside and around the production zones most of those are in the easy to slip region of easy slip. The poles of the fractures inside/around the production zones are concentrated around the area of the lowest critical pore pressure.

be seen in the BHTV image but could be seen in the core from which the in situ stress had been released.

Fig. 16(a) shows the poles to all the fractures detected on the BHTV log, whereas, Fig. 16(b) shows the poles to fractures which lie within and near the producing zones. The latter are considered to contribute to production (i.e. are 'flowing' fractures), and evidently are concentrated around the area of lowest critical pore pressure. Fractures with these orientations can slip most easily at lower pore pressures.

8. Discussion

These results support the notion that the hydraulically conductive fractures in the Hijiori reservoir were formed by the slippage of favorably-oriented, pre-existing, weak joints due to increasing pore pressure, and that flow paths within the reservoir develop along these fractures. This understanding is compatible with the insight of Sibson (1996) who introduced Hill's mesh model (Hill, 1977) to explain a mesh structure in which strong directional permeability may develop in the δ_2 direction, parallel to fault-fracture intersections, as is illustrated in Fig. 17(a). Hill's mesh was conceived as a model for earthquake swarms and involved the migration of fluids through a 'honeycomb' mesh of interlinked minor shear fracture and extension fractures. The microseismic activity at the Hijiori reservoir induced by the hydraulic injections may be analogous to earthquake swarms arising from natural overpressurization. The generic mechanism of the induced microseismic events and the earthquake swarms are similar. In the Hijiori case, however, the character of the microseismic distributions is planar rather than volumetric. This difference might be explained by heterogeneity in the distribution of pre-existing fractures. The mesh structure is regarded as consisting of interlinked extensional fractures and conjugate shear fractures. If a distribution of pre-existing fractures is biased toward one of the conjugate orientations of shear failure, a structure

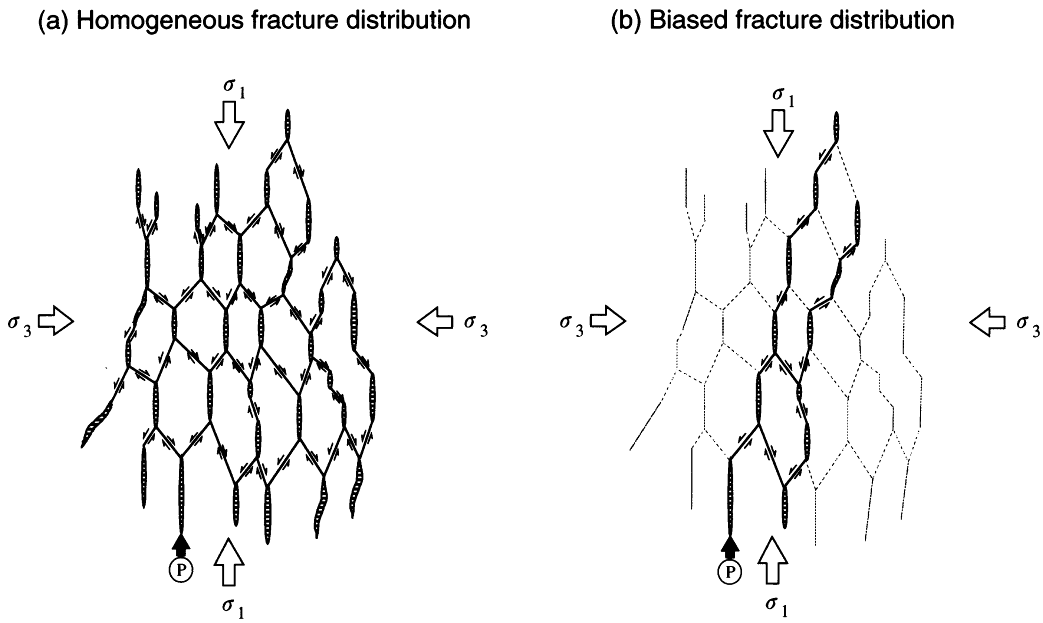

Fig. 17. The Hill (1977) mesh model for earthquake swarms triggered by the migration of fluids through a 'honeycomb' mesh of interlinked minor shear fracture and extension fractures. Strong directional permeability may develop in the nine directions parallel to the fault-fracture intersections. The mesh tends to be volumetric if a distribution of pre-existing joints is homogeneous (a). However, the mesh becomes planar if a distribution of pre-existing joints is biased toward one of the conjugate orientation of shear failure (b).

will tend to develop toward that direction, as shown in Fig. 17(b).The biased structure is planar rather than volumetric.

In the Hijiori reservoir, the maximum principal stress is nearly vertical (slightly tilting to the east), and the minimum is sub-horizontal and oriented north–south. Therefore, the two sets of conjugate orientations for shear failures are toward the SSE with low-to-medium inclination and the NNW with low inclination as shown in Fig. 16. However, most of the poles of BHTV-imaged fractures are concentrated in one of the conjugate orientation; that is, toward the SSE with low-to-medium inclination. In view of this, it is inferred that the planar character of the microseismic distribution was a consequence of the interaction of the biased distribution of the fracture system with the stress field.

9. Conclusions

We have examined the utility of microseismic cluster analysis as a tool for estimating the in situ stress field, and applied it to estimate the stress state at the Hijiori HDR test site, Japan. We found that individual events within a cluster tended to lie on a plane, and that this plane coincided with one of the focal planes of the focal mechanism solution of the events in the cluster. This provides a basis to recognize the common plane as that on which slip actually occurred. The ensemble of data on slip planes and slip vectors were then inverted to obtain the stress state using an adaptation of Hayashi and Masoka's (1995) method. The results were consistent with stress estimates derived from other sources, such as the microseismics focal mechanisms (Sasaki and Kaieda, 1998) and BHTV images (Okabe et al., 1995).

The mechanics of permeability creation within the reservoir during major hydraulic injections was then examined by evaluating the interaction of the inferred stress field with the natural fracture system. The characteristics of the latter were determined by integrating information obtained from core samples, BHTV images and PTS logs. The relationship between these items is explained well on the basis of Coulomb friction theory. The results can be summarized as follows:

- Flow paths are mainly created by shear slippage along pre-existing fractures provoked by elevated pore fluid pressure.
- Fractures which contribute to fluid production tend to be favorably oriented for shear failure; that is, their orientation is such that the condition for Coulomb failure is reached for the smallest pore pressure increase.
- The growth direction of the reservoir is strongly controlled by the distribution of favorably oriented pre-existing fractures and their interaction with the stress field.

It is concluded that the important factor which characterizes the growth of an artificial HDR reservoir is the interaction between the stress field and suitably oriented fractures. This conclusion highlights the importance of determining the stress field and the characteristics of the pre-existing fracture population when designing the creation of an artificial reservoir.

Acknowledgements

The authors would like to thank Keith F. Evams for his valuable comments and discussions to modify the manuscript and New Energy and Industrial Technology Development Organization (NEDO) for permission to use their data. This research was carried out as a part of the MTC (More Than Cloud) international collaborative project supported by NEDO, Japan (International Joint Research Grant).

References

Augliera, P., Cattaneo, M., Eva, C., 1994. Seismic multiplets analysis and its implication in seismotectonics. Tectonophysics 248, 219–234.

Barton, C.A., Peska, P., Zoback, M.D., 1997. Utilizing wellbore image data to determine the complete stress tensor: application to permeablity anisotoropy and wellbore stability. The Log Analyst November–December, 21–33.

Gephart, J.W., Forsyth, D.W., 1984. An improved method for determining the regional stress tensor using earthquake focal mechanism data: application to the San Fernando earthquake sequence. J. Geophys. Res. 89, B11, 9305–9320.

Hayashi, K., Masoka, M., 1995. Estimation of tectonic stress from slip data obtained from fracture in core samples. In:

Proc. Int. Workshop on Rock Stress Measurement at Great Depth, pp. 35–39.

Hill, D.P., 1977. A model for earthquake swarms. J. Geophys. Res. 82 (8), 1347–1352.

Kitani, S., Tezuka, K., Yagi, M., Miyairi, M., 1998. Geologic structure in and around Hijiori HDR test site. Draft proceedings. In: 4th Int. HDR Forum Strasbourg.

Moriya, H., Niitsuma, H., 1994. Determination of subsurface stress direction by means of AE doublet source location and focal mechanism analysis. Progress in Acoustic Emission 7, 481–486.

Moriya, H., Nagano, K., Niitsuma, H., 1994. Precise source location of AE doublets by spectral matrix analysis of triaxial hodogram. Geophysics 59, 36–45.

Okabe, T., Shinihara, N., Takasugi, S., Hayashi, K., 1995. Stress analysis of induced fractures by inversion method (Part 2) — application to field data. In: Proceedings of the 92nd SEGJ Conference, pp. 11–15.

Parker, R.H., 1989. In: Hot Dry Rock Geothermal Energy: Phase 2B Final Report of the Camborne School of Mine Project vol. 1. Pergamon Press.

Phillips, S.W., House, L., Fehler, M., 1997. Detailed joint structure in a geothermal reservoir from studies of induced microearthquake clusters. Journal of Geophysical Research 102, 11745–11763.

Pine, R.J., Batchelor, A.S., 1984. Downward migration of shearing in jointed rock during hydraulic injections. Int. J. Rock Mech. Min. Sci. Geomech. Abstr. 21 (5), 249–263.

Poupinet, G., Ellsworth, W.L., Frechet, J., 1984. Monitoring of velocity variations in the crust using earthquake doublets: an application to Calaveras Fault, California. Journal of Geophysical Research 89, 5713–5719.

Sasaki, S., Kaieda, H., 1998. Stress state at the Hijiori HDR site inferred from focal mechanism data. In: 4th Int. HDR Forum Strasbourg.

Sibson, R.H., 1996. Structural permeability of fluid-driven fault-fracture meshes. Journal of Structural Geology 18 (8), 1031–1042.

Tezuka, K., Niitsuma, H., 1995. Microseismic doublet analysis for fracture characterization in Hijiori HDR test site. In: Proceedings of 3rd SEGJ/SEG International Symposium Geotomography — Fracture Imaging, pp. 148–155.

Walsh, J.B., Grosenbaugh, M.A., 1979. A new model for analyzing the effect of fractures on compressibility. Journal of Geophysical Research 84, 3532–3536.